**Proceedings of the ASME 2021 40th International Conference on Ocean, Offshore and Arctic Engineering**
**OMAE2021**
**June 21-30, 2021, Virtual, Online**

**OMAE2021-62288**



# ON UNCERTAINTY ASSESSMENT OF FATIGUE DAMAGE OF PROPULSION SHAFT UNDER ICE IMPACT

**Etienne Purcell, Amir R. Nejad**
Department of Marine Technology
Norwegian University of Science & Technology
Trondheim, Norway, NO-7491
Email: etienne.purcell@ntnu.no

**Mostafa Valavi**
EDR & MEDESO AS
Lysaker
Norway

**Anriëtte Bekker**
Department of Mechanical
& Mechatronic Engineering
Stellenbosch University
Stellenbosch, South Africa, 7600

## ABSTRACT

*In this paper, the importance of maintenance of marine propulsion is discussed with specific focus on the use of condition monitoring to inform maintenance schedules. The design requirements of DNV GL for shafts expected to operate in ice infested waters is adapted and a method is proposed to calculate the short-term fatigue damage during ice impacts. This method uses the Palmgren-Miner rule to calculate fatigue damage based on a transient, lumped-mass model simulation of the shaft with ice loads calculated from shaft measurements using inverse methods. Relevant sources of uncertainty in this assessment method are identified and quantified in order to express the short-term fatigue damage in a stochastic form. Sources of uncertainty include uncertainty in the calculation of ice loads, uncertainty of the transient analysis and uncertainty regarding the actual failure of the shaft as predicted by the S-N material curve and the Palmgren-Miner method. Uncertainties that influence the stress history are found to be the greatest contributor to fatigue damage uncertainty. A method is discussed that calculates the remaining useful life of the shaft as a function of short-term fatigue damage and the identified sources of uncertainty. The S.A. Agulhas is used as a case study to quantify the fatigue damage.*

## 1 INTRODUCTION

The function of a ship is intrinsically dependant on the proper functioning of the propulsion system. DNV GL identifies the propulsion system as one of the main functions of a vessel [1] with several safety requirements aimed at ensuring the availability of propulsion functions [2]. Even though shipping incidents have decreased in recent years, machinery damage or failure, comprising partially of propulsion failure, has been the greatest cause of shipping incidents during the last decade [3]. The greatest concerns of propulsion loss is the possibility of collisions and grounding with far reaching monetary, ethical and social perception effects for the ship owner or operator [4].

Maintenance strategies are described by the International Orginization for Standardization (ISO) [5] and the International Association of Classification Societies (IACS) through classification societies such as DNV GL [6] in order to limit the probability of propulsion failure. This approach is however not infallible with the greatest contributor to loss of propulsion identified as insufficient maintenance of the propulsion systems [4].

A case study of the marine industry has shown that maintenance is primarily conducted on a scheduled basis with intervals determined by the manufacturers of the components or by the minimum regulatory requirements [7]. Tomlinson [8] and Eisinger [9] agree that the trend in the maritime industry is towards condition based maintenance. This is also evident in the allowance by classification bodies to amend maintenance schedules based on measurements of key metrics [10, 11].

A term that is often associated with predictive maintenance

*Address all correspondence to this author.

is condition monitoring (CM). The outputs of the condition monitoring process can be used to inform the correct maintenance intervals for monitored components.

Condition monitoring is a set of methods used to measure and trend characteristic parameters of a system in order to predict the deteriorating condition of the system [12]. Typical parameters used to monitor the condition of marine propulsion systems include vibration, oil particle density, temperature and electric current [5, 8].

Of particular interest for the current work is the process in which past data is used to predict the future condition of the measured parameter in order to determine the time until failure is expected. The time from the present to the time of expected failure is often called the remaining useful life (RUL) of a component or system. The process of prognosis is extrapolative in nature and is sensitive to uncertainty. For this reason, the RUL is expressed in terms of a confidence level that is a percentage value which denotes the amount of certainty that the prognosis is correct [13]. The uncertainty present in the methods used to calculate the RUL has to be known in order for the total uncertainty to be calculated.

Loads exerted on the shaft of ships are generally a combination of torque which drives the rotation of the propeller, bending moments due to forces on the propeller and missalignment and finally axial thrust due to the hydrodynamic lift of the propeller [14]. The failure of shafts is dominated by fatigue failure with special consideration required for transient conditions such as torsional vibration as a result of engine miss-fire or propeller-ice impacts [15].

As a step towards the implementation of a digital twin platform for the condition monitoring of the polar supply and research vessel, S.A. Agulhas II, the current work will aim to identify relevant sources of uncertainty present in the calculation of fatigue damage due to ice impacts. The sensitivity of the fatigue damage to these uncertainties is quantified followed by a description of how the RUL can be formulated.

## 2 METHODOLOGY

In this paper, a method for the calculation of fatigue damage due to ice impacts that accounts for uncertainty is proposed. This is done by discussing how ice loads are calculated through inverse methods (§ 3), how shaft response to ice loads can be simulated (§ 4) and how these responses can be used to calculate fatigue damage during operation (§ 5). Sources of uncertainty in this method is then identified and quantified (§ 6) and used to define a method for the calculation of the RUL (§ 7). This method is illustrated in Fig. 1.

## 3 ICE LOADS

In order to calculate shaft response and fatigue damage, the loads on the system have to be known. These loads include the ice induced torque, bending and axial loads. Fatigue due to ice is dominated by torsional rather than bending stresses on the majority of the shaft [16]. For this work, only torsional effects of ice loads are considered. This section will describe the design ice load cases (according to [17]) and discuss how ice loads can be calculated during operation. For clarity, ice impacts refer to a single propeller blade impacting on a block of ice, while ice loads will be used to refer to all impacts on a single block of ice and includes milling of the ice.

### 3.1 DNV GL ice loads

Torsional ice loads are modelled as a series of ice impacts mainly to ensure that ice milling does not result in resonance of the shaft [17]. The time-series of each ice impact is described with half sinusoidal function dependant on the shaft rotation angle ($\phi$) as shown in Eq. 1 [17]. The parameters of this function ($C_q$ and $\alpha_i$) are adjusted to simulate different ice impact conditions and are dependant on the number of propeller blades. Four different ice loads are described in the latest DNV GL documents and consists of a fixed number of ice impacts on each blade which are shifted by a prescribed time increment and with the ice load modelled as the sum of the ice impacts [17].

$$Q_{ice}(\phi) = \begin{cases} C_q \cdot Q_{ice,max} \sin\phi \frac{180}{\alpha_i}, & \text{if } 0 \leq \phi \leq \alpha_i \\ 0, & \text{if } \alpha_i \leq \phi \leq 360 \end{cases} \quad (1)$$

### 3.2 Operational ice loads

The ideal method to determine loads at the propeller is through direct measurements. This is however not practically possible due to harsh operating conditions and high costs [18]. Recent studies have aimed to develop methods that allow for measurements on accessible areas of the shaft to be used to calculate ice loads. These methods have however not been verified with full-scale or model-scale experiments.

Ikonen et al. [19] and De Waal et al. [20] have shown that ice loads can be calculated through the regularisation of an ill-posed inverse problem. The method allows for short time signals of ice-induced torque to be calculated from strain measurements at a location between the propeller and the motor. Even though different methods of regularisation are possible, ice loads predicted using the Truncated Generalized Singular Value Decomposition method predicts the greatest peak ice torque and can be used for fatigue damage prediction [20]. These methods do not account for motor control response or the changes in hydrodynamic torque resulting from the decrease of propeller speed during ice impacts.

Polić et al. [18] has developed an inverse method that uses modal decomposition of the shaft to calculate the ice-induced propeller torque using rotational speed and angular deformation measurements on the propeller shaft while ignoring the effect of

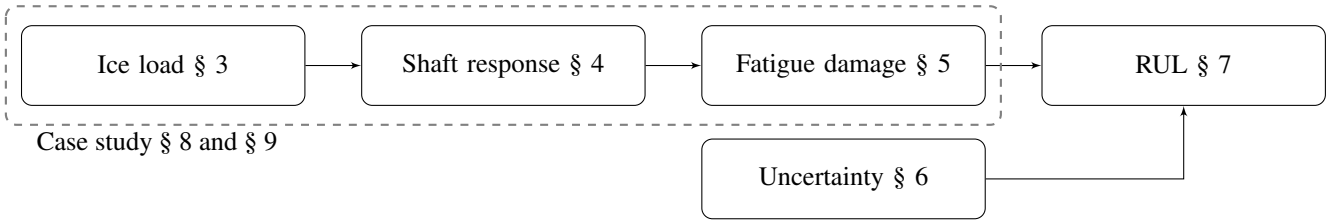


**FIGURE 1**: RUL methodology

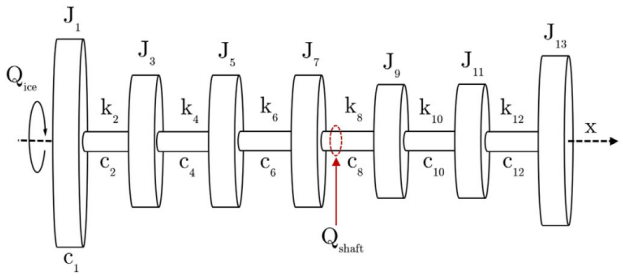


**FIGURE 2**: LUMPED-MASS MODEL OF THE SHAFT [20]

damping of the shaft. This method is preferable as it accounts for changes in hydrodynamic torque as well as motor control response by including allowance for shaft speed measurements.

## 4 TRANSIENT SHAFT RESPONSE

In order to calculate the transient response along the length of the shaft, the shaft can be simulated. Various methods can be used including multi-body simulation, finite element simulation and energy based methods such as bond graphs. DNV GL recommends the use of a lumped-mass model for the torsional behaviour of shafts [15]. This results in a set of differential equation which can be solved in the time domain using numeric integration techniques such as the Newmark-Beta method [19, 20]. This method allows for simulations that require less computational power to solve than high-fidelity simulations. The use of a reduced order model generated from a high-fidelity model is however also a viable solution for real-time transient simulations.

A lumped-mass model of the shaft of the S.A. Agulhas II is shown as an example in Fig . 2. This model was used for the inverse calculations described previously (§ 3). Here $Q_{ice}$ is the ice torque, $Q_{shaft}$ is the measured shaft torque, $k$ is the stiffness of the shaft, $c$ is the water and shaft damping and $J$ is the inertia elements of the shaft.

## 5 FATIGUE DAMAGE

If the transient response of the shaft is known at all locations, the fatigue damage can be calculated along the length of the shaft. This section will describe how design calculations account for fatigue and how this can be modified for the monitoring of fatigue damage during operation.

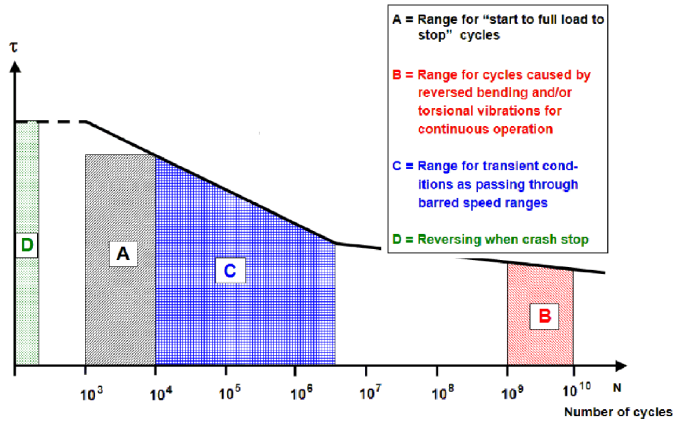


**FIGURE 3**: LOAD CASES CONSIDERED FOR SHAFT FATIGUE IN DNVGL-CG-0038 SHOWING STRESS AND APPLICABLE NUMBER OF CYCLES (ADAPTED FROM [15])

### 5.1 DNV GL shaft fatigue calculations

For DNV GL classed vessels, two possible methods are allowed to calculate the load-carrying capacity of shafts. A simplified, conservative method which calculates the minimum shaft diameter [21] or a a fatigue analysis based on the S-N curve of the shaft material [15]. The method using the fatigue approach will be discussed further.

The fatigue calculations are simplified by the assumption that the fatigue life of the shaft is only dependant on torsional and bending loads. Additionally, the full spectrum of loads are not considered, but the guidelines only consider load cases which are deemed as dominant and prescribes a minimum safety factor for these load cases. The typical load cases considered are shown in Fig. 3. This includes allowance for high-cycle fatigue and low-cycle fatigue.

Low-cycle fatigue is focused on the stress range caused by variation in torsion between zero and full load of the shaft without consideration of rotational effects that vary according to the shaft speed [15]. Ice loads are accounted for by the increase of the full load by the peak ice load.

High-cycle fatigue calculations are relevant to loads with more than $3 \cdot 10^6$ repetitions and consists of a combination of torsional vibration and bending stresses due to rotation [15]. Typically, loads that contribute to this includes engine firing pulses, changes in hydrodynamic forces, ice impacts as well as bending due to whirling, miss-alignment and hydrodynamic drag on exposed portions of slanted shafts [15, 21]. The basic method for design against high cycle fatigue failure is dependant on the nominal vibratory torque ($\tau_v$), the nominal bending stress ($\sigma_b$), the safety factor ($S$) and the high cycle fatigue strength against torsion ($\tau_f$) and bending ($\sigma_f$) with the relationship shown in Eq. 2 [21]. The fatigue strength values $\tau_f$ and $\sigma_f$ are dependant on material properties, geometry of the shaft and mean loads.

$$\left(\frac{\tau_v}{\tau_f}\right)^2 + \left(\frac{\sigma_b}{\sigma_f}\right)^2 \leq \frac{1}{S^2} \tag{2}$$

Typically, shaft failure occurs at locations of stress concentration such as holes, changes in diameter and keyways [14, 15, 22]. Geometric stress concentration factors are a way to quantify the point of highest stress due to the change in stress field resulting from a discontinuity in the geometry of the shaft. The DNV GL guidelines provide tables and equations to quantify this effect for a set of common shaft geometries such as keyways, radial holes, splines and diameter changes [15].

### 5.2 Palmgren-Miner linear damage rule for fatigue

The methods described previously are however only designed to ensure that the shaft is able to withstand a pre-defined amount of cycles with limited applicability to condition monitoring. The Palmgren-Miner linear damage rule for fatigue, combined with rainflow cycle counting, will be described as a means to achieve condition monitoring.

The Palmgrem-Miner method calculates the cumulative damage of fatigue ($D$) using Eq. 3. To accomplish this, the stress history is divided into $k$ stress values with magnitude $S_i$. The ratio between the amount of cycles ($n_i$) and the number of cycles that would cause failure at that stress level ($N_i$) is calculated for each stress value. The sum of these ratios are calculated and fatigue failure is predicted when the cumulative damage over the life of a component ($D = 1$). A safety factor can be incorporated by decreasing the limit of cumulative damage proportionally [23].

$$D = \sum_{i=1}^{k} \frac{n_i}{N_i} \tag{3}$$

The number of cycles that results in failure at each stress level is calculated as shown in Eq. 4. The constants $K_c$ and $m$ are material dependant and can be obtained from the S-N curve of the material. Stress-concentration factors can be included by adjusting the S-N curve or by increasing the stress history.

$$N_i = K_c \cdot S_i^{-m} \tag{4}$$

The shaft stresses are in reality a combination of bending and torsional stress [15] and these components can be combined for use in Eq. 4. Possible stress theories that can accommodate various stress components include the von Mises and the Tresca methods [24]. Tests have shown that the results predicted using the von Mises theory correlates well with experimental results for combined bending and torsional loading [25]. As stated previously, this work considers the effects of bending stress to be negligible.

DNV GL provides requirements for the use of the Palmgren-Miner method [16]. The cumulative damage limit is set to one ($D \leq 1$) as the factors included in the calculation of the fatigue limits are deemed to be sufficiently conservative [16]. A minimum of 10 stress bins are required and the material S-N curve is described by a bi-linear logarithmic function described by Eq. 5 with material parameters calculated from the high cycle fatigue limit ($\tau_{vHC}$) low cycle fatigue limit ($\tau_{vLC}$) and the torsional fatigue strength ($\tau_f$) at $1 \cdot 10^9$ cycles as shown in Eq. 6 to Eq. 9 [16]. The material constants are calculated using the material strength, geometrical stress concentration factors, notch sensitivity factors, surface roughness and safety factors [15]. In order to model the long-term fatigue due to ice impacts, the stress distribution is modelled with a two-parameter Weibull distribution [16, 17].

$$N = \begin{cases} K_1 \cdot \tau^{-m_1}, & \text{if } N \leq 3 \cdot 10^6 \\ K_2 \cdot \tau^{-m_2} & \text{otherwise} \end{cases} \tag{5}$$

$$m_1 = \frac{2.477}{\log(\frac{\tau_{vLC}}{\tau_{vHC}})} \tag{6}$$

$$m_2 = \frac{2.523}{\log(\frac{1.5 \cdot \tau_{vHC}}{\tau_f})} \tag{7}$$

$$K_1 = 3 \cdot 10^6 \cdot {\tau_{vHC}}^{m_1} \tag{8}$$

$$K_2 = 3 \cdot 10^6 \cdot {\tau_{vHC}}^{m_2} \tag{9}$$

## 6 MODEL UNCERTAINTY

Up to this point, this work has described fatigue damage as deterministic. In order to provide meaningful condition monitoring solutions that provide RUL estimations with acceptable accuracy, the uncertainty of the predicted fatigue damage has to be considered [13]. Uncertainty is a measure of the confidence that a value will lie within a certain range of values [26] and is commonly expressed as normal, log-normal and Weibull distributions. These distributions ($\chi$) can be calculated as the ratio between the actual value ($X_{actual}$) of a parameter and the pre-

dicted value ($X_{model}$) as shown in Eq. 10 [27]. In order to approximate the actual value, large amounts of experimental data or high-accuracy models are required. This formulation allows for uncertainties to be considered independently with mean values close to, or equal to, 1.

$$\chi = \frac{X_{model}}{X_{actual}} \tag{10}$$

For the sake of RUL estimation, three types of uncertainties should be considered including present uncertainty (sensor accuracy and filter effect), future uncertainty (future loads and extrapolation methods) and modeling uncertainty (simplifications of system behaviour) [28].

This section will identify relevant sources of modeling uncertainty in the calculation of fatigue damage due to ice loads. Some uncertainties are quantified from literature while the need for future work is identified for the remaining sources. The distributions used to model the uncertainties are shown in Tab. 1.

### 6.1 Ice load calculation ($\chi_{inv}$)

This is the uncertainty associated with the time history of the ice loads. As stated previously, the actual value has to be known to calculate uncertainty. The inverse methods to calculate ice loads was however created out of necessity as the actual ice torques are difficult to measure [18]. In order to quantify the errors present in the method utilised by De Waal et al. [20], two torque measurements were used to calculate two time series of the ice torque which were compared [29]. The results indicated that there was slightly less than 95% correlation, but that there was significant discrepancy between the peak torque predicted.

Polić et al. [18], using the method of modal superposition, defined acceptable limits for the difference between the inversely calculated and simulated ice loads. These limits dictate that 95% of normalised residuals should be within 10% to either side of zero. This is similar to a normal distribution with a standard deviation of 0.05. The uncertainty was found to be influenced by the location of measurement as well as the sampling rate of the measured strain and rotational speed.

There are however no model-scale or full-scale data available to evaluate the actual model uncertainties. The need for further research is identified that quantifies the uncertainty of the different methods used to calculate ice loads.

For the purpose of this paper, the correlation calculated by Nickerson et al. [29] and the acceptable error bounds used by Polić et al. [18] is used to assume a lognormal distribution with a variance of 0.05 for the use of inverse methods to calculate ice loads.

### 6.2 Lumped mass model ($\chi_{mod}$)

The lumped-mass model is a simplification of the actual system and introduces some uncertainty for the benefit of shorter simulation time. The parameters used for the model, namely the stiffness, inertia and damping values, can vary between the design-stage model and the actual propulsion system [30]. This can result in the over- or underestimation of the torsional vibration response of the shaft [30].

Kardeniz [31] provides a framework for the estimation of model uncertainty due to uncertainty in the parameters of a lumped mass model. The uncertainty of the mass and stiffness values can be evaluated simultaneously using the natural frequencies of the system [31]. In keeping with the example of Kardeniz [31], a coefficient of variance of 0.05 is used for lumped mass models. It is possible to decrease this uncertainty by the tuning of the lumped-mass model to match the natural frequencies of the system or with the use of high-fidelity models.

### 6.3 Temporal response

The behaviour of the shaft is described as a set of differential equations based on the lumped-mass model. These equations are solved with numerical methods which divide the differential equations into a number of finite steps and results in an approximation of the actual solution [32].

The accuracy of the solution is not only dependant on the method used, but also on the step sizes. To evaluate this effect, the simulation of an ice impact can be repeated with decreasing step sizes to determine when convergence is reached. Further work is required to quantify this uncertainty.

### 6.4 Material properties ($\chi_{S-N}$)

The S-N curve of materials are created based on a best-fit approach after testing of a limited number of samples [15] which means that there is some uncertainty present in the exact fatigue life of the shaft material. The material curve is usually created with a pre-defined probability of failure [16].

The results used to calculate the S-N curve is highly dependant on employed experimental methods [16] and is not explicitly stated for DNV GL calculations. Previous studies have however identified that the logarithm of $K$ follows a normal distribution with further work needed to quantify the standard deviation of this distribution [33]. The coefficient of variance was found to fall in the range between 0.05 and 0.035 [33] and an average value of 0.02 seems to be reasonable when no additional information is available.

### 6.5 Palmgren-Miner method ($\chi_{PM}$)

The Palmgren-Miner method has some shortcomings and does not account for the order in which stress cycles occur [16]. This effect and other shortcomings result in possible fatigue failure when the cumulative damage is not equal to 1. The majority of failures occur close to the proposed value of 1 and usually in the range between 0.5 and 2.0 [16]. Some older work has found

**TABLE 1**: MODEL UNCERTAINTY

| Uncertainty | Distribution | Mean ($\mu$) | St. dev. ($\sigma$) |
|---|---|---|---|
| $\chi_{inv}$ | Lognormal | 1.00 | 0.05 |
| $\chi_{mod}$ | Lognormal | 1.00 | 0.05 |
| $\chi_{S-N}$ | Lognormal | 1.00 | 0.02 |
| $\chi_{PM}$ | Lognormal | 1.00 | 0.15 |

that a coefficient of variance of 0.15 is applicable to the Palgrem-Miner method for fatigue calculation in marine structures assuming that failure occurs at $D_c = 1$ [34].

### 6.6 Simplified uncertainty treatment in short-term fatigue

Uncertainties would impact the short-term fatigue damage in different and complex ways. These impacts are however simplified in order to obtain approximate results. The uncertainty of the lumped-mass model response ($\chi_{mod}$) and the inverse methods ($\chi_{inv}$) would change the stress amplitude while the uncertainties of the material properties ($\chi_{S-N}$) and the Palmgren-Miner method would impact the cumulative damage inversely. Combining Eq. 3, Eq. 4 and the model uncertainties results in a stochastic short-term fatigue damage ($D^{ST}$) as shown in Eq. 11. The deterministic short term fatigue due to an ice load ($D_{ice}$) in this case is calculated using the methods described in § 3 to § 5. Once quantified, the uncertainty regarding the temporal response can be treated in the same way as $\chi_{mod}$ and $\chi_{inv}$ as it would also affect the stress component of the equation. The DNV GL calculations account for the uncertainties $\chi_{S-N}$ and $\chi_{PM}$ with the use of safety factors and should not be included if the S-N curve of DNV GL is used.

$$D^{ST} = \frac{(\chi_{mod} \cdot \chi_{inv})^m}{\chi_{S-N} \cdot \chi_{PM}} \sum_{i=1}^{k} \frac{n_i}{N_i} = \frac{(\chi_{mod} \cdot \chi_{inv})^m}{\chi_{S-N} \cdot \chi_{PM}} \cdot D_{ice} \qquad (11)$$

### 6.7 Sensitivity of fatigue damage to model uncertainty

As a means to quantify the sensitivity of the predicted short-term fatigue damage on the model uncertainty, a basic Monte-Carlo simulation is used. This is done by changing the values of a single model uncertainty distribution while keeping the others unchanged and evaluating the change in the average of the stochastic short-term fatigue damage.

The deterministic short-term fatigue damage ($D_{ice}$) was given a fixed value and a set of random data points generated using the distributions given in Tab. 1. A set of values for the stochastic short-term fatigue damage was calculated using the random data and Eq. 11 after which the average of $D^{ST}$ was calculated. The process was repeated with an increase of 1% in the data contained in the random distributions with resulting changes in the average of $D^{ST}$ reported in Tab. 2. The value of $m_1$ as calculated for the case study (§ 9) was used for this calculation.

**TABLE 2**: SENSITIVITY OF FATIGUE DAMAGE TO MODEL UNCERTAINTY

| Uncertainty | Change in $D^{ST}$ mean (%) |
|---|---|
| $\chi_{inv}$ | 7.42% |
| $\chi_{mod}$ | 7.42% |
| $\chi_{S-N}$ | 1.00% |
| $\chi_{PM}$ | 1.02% |

It is clear that the uncertainty of the lumped-mass model and the inverse methods have the greatest influence on the predicted short-term fatigue damage. This is due to the effect of $\chi_{mod}$ and $\chi_{inv}$ being raised to the power of $m$.

## 7 REMAINING USEFUL LIFE PREDICTION

This section will describe how the RUL can be estimated with consideration given to the relevant model uncertainties. The formulation of the prognostic process is based on the work by Sankararaman [28].

In order to calculate the RUL of the shaft, the fatigue damage can be described as a function of discrete increments and is usually formulated as a function of time. For the purpose of fatigue damage due to ice loads the long-term fatigue damage is described as a function of the number of ice loads ($x$) with the RUL consequently calculated as a number of remaining ice loads before failure. This is a simplification that equates $x$ to the time during each ice load. The fatigue damage after an ice load ($D(x+1)$) is a function of the damage before the ice load $D(k)$ and the stochastic short-term fatigue damage ($D^{ST}$) during the ice load as shown in Eq. 12. This means that the fatigue damage at a certain point in time is the sum of all previous short term fatigue damage which corresponds to the Palmgren-Miner approach assuming that zero fatigue damage accumulated between ice loads.

$$D(x+1) = D(x) + D^{ST} \qquad (12)$$

Even though the cumulative damage of the shaft is a physical parameter with a real and fixed value, the real value is unknown and the uncertainty of previous steps should be accounted for resulting in the propagation of the uncertainty which results in difficult to predict distributions of the RUL [28].

Due to the uncertainties present in prognostics, the RUL is stochastic in nature and requires numeric or analytic methods to calculate [28]. An example of a numeric method is the Monte-

Carlo method and an analytical method is the First Order Reliability Method (FORM) [28].

## 8 CASE STUDY VESSEL

In order to demonstrate the application of the initial stages of this method, the S.A. Agulhas II is introduced as a case study. The suitability of this vessel for this case study stems from the availability of inversely calculated torque data during ice impacts [35]. The vessel is classed by DNV GL as Polar Ice Class PC-5 which entails requirements for propulsion strengthening against ice impacts [15, 17, 36].

### 8.1 Shaft specifications

The vessel propulsion consists of two directly coupled systems, each consisting of an electric motor, motor shaft, intermediate shaft, propeller shaft and a controllable pitch propeller. The motor shaft is connected to the intermediate shaft with flanges while the intermediate shaft is connected to the propeller shaft with a rigid coupling [37]. Each motor is rated at 4500 kW and 140 rpm. The maximum design ice torque is 1009.9 kNm.

## 9 CASE STUDY RESULTS

This section will describe the results obtained for the short-term fatigue damage for a small sample of ice loads.

### 9.1 Critical fatigue locations

This section will consider the shaft of the S.A. Agulhas II in order to identify critical locations that should be considered for fatigue calculations.

Simulations of ice impact show that the peak torque is similar along the length of the shaft. This matches with the simulation results of Polić et al. [18]. This means that the location on the shaft with the greatest nominal shear stress will be governed by shaft geometry.

The torsional stress is inversely proportional to the polar moment of inertia ($W_t$) and directly proportional to the radius ($r$) of the shaft at the area which is considered ($\tau = {}^{T \cdot r}/_{W_t}$) [15, 38] and the stress would be greatest at the outer radius ($r_o$) of the shaft. The ratio ${}^{r_o}/_{W_t}$ is calculated for each of the sections of the shaft and shown with the inner ($d_i$) and outer diameters ($d_o$) in Tab. 3. The section numbers correspond to each of the shaft sections used in the lumped-mass model as shown in Fig. 2.

The transient vibration analysis in the design documentation is limited to the stresses on section 12, the motor shaft. The focus of the design documents along with the results shown in Tab. 3 indicates that this area is the primary concern for fatigue condition monitoring. For the remainder of this section, it is assumed that the critical fatigue location is on the motor shaft.

**TABLE 3**: CRITICAL LOCATIONS FOR TORSIONAL STRESS ON THE SHAFT

| Section | $d_o$ [m] | $d_i$ [m] | $r_o/W_t$ [m$^{-3}$] |
|---|---|---|---|
| 2 | 0.5 | 0.125 | 40.9 |
| 4 | 0.5 | 0.125 | 40.9 |
| 6 | 0.5 | 0.125 | 40.9 |
| 8 | 0.5 | 0 | 40.7 |
| 10 | 0.5 | 0 | 40.7 |
| 12 | 0.4 | 0 | 79.6 |

There is a stress riser on the motor shaft in the form of a machined flange. Assuming a multi-radii transition, the geometric stress concentration factor at this location is equal to 1.05. Approximating the dimensions of the flange and radius from the design drawing results in a factor of 1.61. The more conservative factor of 1.61 is used for the fatigue damage calculation.

### 9.2 Transient shaft simulation

The response of the shaft is calculated with the lumped-mass model shown in Fig. 2 as per the recommendations of DNV GL [16]. The model is created in Ansys Twin Builder using system parameters according to the design documentation [20, 39]. The temporal solution is calculated using the Adaptive Trapezoid-Euler iterative method.

The sum of the hydrodynamic torque and the ice torque is applied to the propeller ($J_1$ in Fig. 2) and the motor torque is applied to the rotor ($J_{13}$ in Fig. 2). Hydrodynamic torque is modelled as proportional to the square of the rotational speed and thus includes water damping effects [16]. The motor is assumed to be operating at rated conditions as required by the ice load calculations [16]. A set of 4 DNV GL ice load cases (as shown in Fig. 4) and 5 ice load cases as reported by de Waal [35] (as shown in Fig. 5) are used as the set of ice loads. DNV GL ice loads are denoted as $Q_{ice_1}$ to $Q_{ice_4}$ and the inversely calculated ice loads are denoted as $Q_{ice_5}$ to $Q_{ice_9}$.

A simulation of 17 seconds is used with the ice impact at 12 seconds. The first 10 seconds is discarded to remove any transient effects during startup of the simulation. This results in a 7 second torque history (similar to the design documents [39]) for each load case. The ice loads for DNV GL case 4 and the associated shaft response are compared in Fig. 6.

Two load cases, DNV GL case 2 ($Q_{ice_2}$) and case 4 from de Waal ($Q_{ice_8}$) [35] results in the motor speed to decrease to zero and predicts that the motor stops. Additional work is required to more accurately model the motor response (currently modelled as the characteristic speed-torque curve as per [39]) to account for this effect.

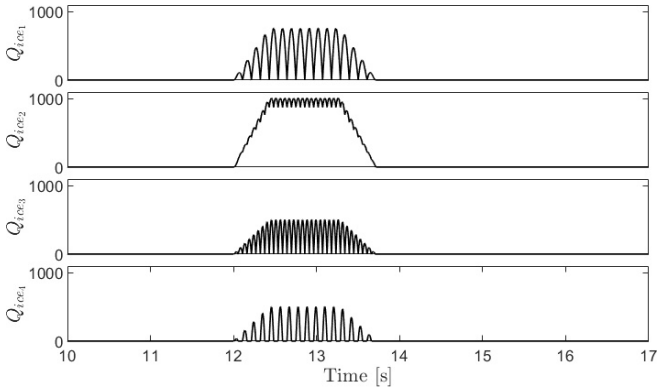


**FIGURE 4**: DNV GL ICE LOADS

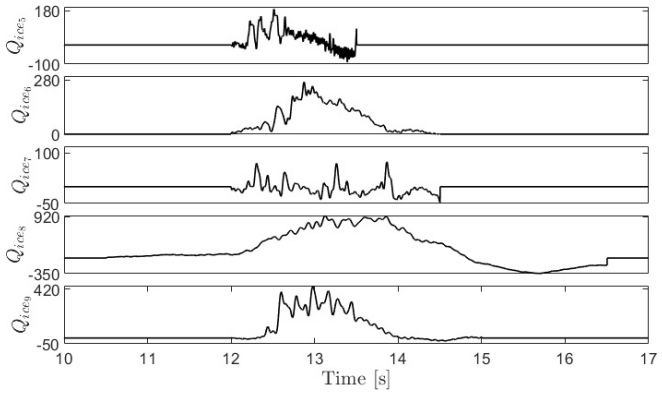


**FIGURE 5**: OPERATIONAL ICE LOADS (ADAPTED FROM [35])

### 9.3 Short-term fatigue damage

The time series response at the critical point is extracted from Ansys Twin Builder and imported into Matlab where the short-term fatigue is calculated. The parameters used in the calculation are given in Tab. 4. In order to calculate the parameters, assumptions are made regarding the yield strength of the material (assumed as $0.6 \cdot S_{UT}$) and the surface roughness.

The short-term fatigue damage ($D_{ice}$) is listed in Tab. 5. The number of cycles for each of the stress ranges for DNV GL case 4 is shown in Fig. 7 as an example of the output of the rainflow cycle counting process. The stress cycles below 3 MPa are omitted in Fig. 7 for the sake of clarity.

The results indicate that the inversely calculated ice loads predict lower fatigue damage when compared to the DNV GL ice loads in most cases. The sample size is however limited and does not allow for conclusions to be made regarding the correlation between the design loads and the operational loads. There is also no clear correlation between the peak ice torque and the resulting fatigue damage on the shaft.

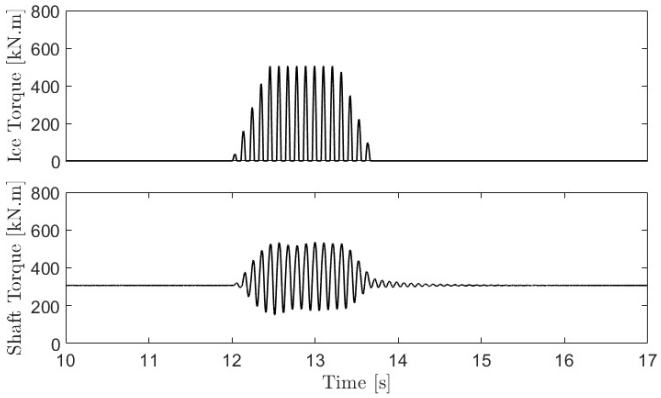


**FIGURE 6**: SIMULATED ICE TORQUE AND SHAFT RESPONSE FOR DNV GL CASE 4 ($Q_{ice_4}$)

**TABLE 4**: PARAMETERS FOR SHORT-TERM FATIGUE DAMAGE CALCULATION

| Parameter | Value |
|---|---|
| Mean shear stress | 24.43 MPa |
| $d_o$ | 0.4 m |
| $W_i$ | 0.0025 $m^4$ |
| $\alpha_t$ | 1.62 |
| $m_1$ | 7.33 |
| $log(K_1)$ | 19.05 MPa |
| $m_2$ | 90.01 |
| $log(K_2)$ | 160.88 MPa |

## 10 CONCLUSION

This paper considers sources of uncertainty relevant to the calculation of short-term fatigue damage on a propulsion shaft during ice impacts. These uncertainties are incorporated into the Palmgren-Miner method in order to find a formulation for fatigue damage that incorporates uncertainty. This is done through firstly identifying a suitable method to calculate fatigue damage, secondly by identifying and quantifying sources of uncertainty, thirdly calculating the relative importance of each uncertainty and finally by describing how the RUL can be calculated. The S.A. Agulhas II is used as a case study to which this method is applied.

A lumped-mass model is used to calculate the transient response of the shaft and the Palmgren-Miner method is used to calculate short-term fatigue damage during ice loads. Limitation of this method includes the consideration of only torsional loads and the use of a simplified motor model that does not account for high frequency excitation caused by the motor.

**TABLE 5**: SHORT-TERM FATIGUE DAMAGE FOR SINGLE ICE IMPACTS

| Load case | Peak torque [kN.m] | $D_{ice}$ |
|---|---|---|
| $Q_{ice_1}$ | 757 | $5.4 \cdot 10^{-7}$ |
| $Q_{ice_2}$* | 1010 | $2.1 \cdot 10^{-9}$ |
| $Q_{ice_3}$ | 505 | $2.3 \cdot 10^{-11}$ |
| $Q_{ice_4}$ | 505 | $5.8 \cdot 10^{-8}$ |
| $Q_{ice_5}$ | 189 | $2.8 \cdot 10^{-12}$ |
| $Q_{ice_6}$ | 270 | $3.1 \cdot 10^{-13}$ |
| $Q_{ice_7}$ | 74 | $3.4 \cdot 10^{-15}$ |
| $Q_{ice_8}$* | 942 | $2.3 \cdot 10^{-8}$ |
| $Q_{ice_9}$ | 443 | $4.5 \cdot 10^{-10}$ |

* Incomplete simulation

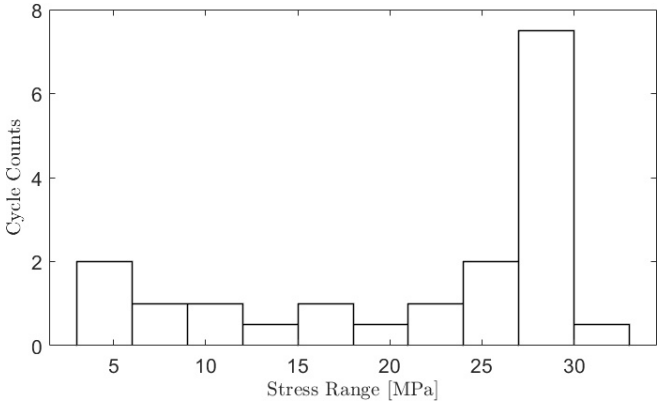


**FIGURE 7**: CYCLES CALCULATED THROUGH RAINFLOW COUNTING FOR DNV GL CASE 4

Identified sources of uncertainty includes the lumped-mass model parameters, the use of a discretized temporal simulation, the inverse calculation of ice loads and the use of the Palmgren-Miner and S-N curve methods.The uncertainties are expressed as lognormal distributions. Uncertainties that influence the stress history has the greatest contribution to fatigue uncertainty.

Future work will include the quantification of the remaining model uncertainties, the use of improved inverse methods, shaft models and motor models. Finally, this work will be used as a module that will be incorporated into a digital twin of the propulsion system of the S.A. Agulhas II.

## ACKNOWLEDGMENT

The authors would like to acknowledge the financial support from MarTERA - an ERA-NET Cofund scheme of Horizon 2020 of the European Commission - and the Research Council of Norway (Project no. 311502).

## REFERENCES

[1] DNV GL, 2020. Rules for classification: Part 1 General regulations, Chapter 1 General regulations. Accessed November 27, 2020, https://rules.dnvgl.com/docs/pdf/DNVGL/RU-SHIP/2020-07/DNVGL-RU-SHIP-Pt1Ch1.pdf.

[2] DNV GL, 2020. Rules for classification: Part 4 Systems and components, Chapter 1 Machinery systems, general. Accessed November 27, 2020, https://rules.dnvgl.com/docs/pdf/DNVGL/RU-SHIP/2018-01/DNVGL-RU-SHIP-Pt4Ch1.pdf.

[3] Allianz Global Corporate & Specialty (AGCS), 2020. Safety and shipping review 2020.

[4] The London P & I Club, TMC Marine, and Bureau Veritas, 2018. Reducing the risk of propulsion loss: Operational guidance for preventing blackouts and main engine failures. Accessed December 17, 2020, https://www.londonpandi.com/media/2141/a-bilbroughcom-profiles-ms_profiles-somesh-desktop-bv_propulsionloss_11x16_0912-web.pdf.

[5] ISO 13613, 2011. Ships and marine technology – Maintenance and testing to reduce losses in critical systems for propulsion.

[6] International Association of Classification Societies, n.d.. About iacs. Accessed November 27, 2020, http://www.iacs.org.uk/about/.

[7] Johansen, S. S., and Nejad, A. R., 2019. "On digital twin condition monitoring approach for drivetrains in marine applications". In Proceedings of the ASME 2019 38th International Conference on Ocean, Offshore and Arctic Engineering.

[8] Tomlinson, N. A., 2016. "What is the ideal maintenance strategy? A look at both MoD and commercial shipping best practice". In Proceedings of the 13th international naval engineering conference and exhibition.

[9] Eisinger, S., and Angelsen, S., n.d.. Prognostic maintenance: seeing intor the future. Accessed December 18, 2020, https://www.dnvgl.com/to2030/technology/prognostic-maintenance-seeing-into-the-future.html.

[10] DNV GL, 2020. Rules for Classification: Part 7 Fleet in service, Chapter 1 Survey requirements for fleet in service. Accessed November 27, 2020, https://rules.dnvgl.com/docs/pdf/DNVGL/RU-SHIP/2020-07/DNVGL-RU-SHIP-Pt7Ch1.pdf.

[11] American Bureau of Shipping, 2020. Rules for sur-

vey after construction, Part 7. Accessed December 18, 2020, https://ww2.eagle.org/content/dam/eagle/rules-and-guides/current/generic/Generics_2020/part-7-july20.pdf.
[12] ISO 17359, 2018. Condition monitoring and diagnostics of machines – General guidelines.
[13] ISO 13381-1, 2015. Condition monitoring and diagnostics of machines – prognostics – part 1: General guidelines.
[14] Vizentin, G., Vukelić, G., and Srok, M., 2017. "Common failures of ship propulsion shafts". *Pomorstvo,* ***31***(2), pp. 85–90.
[15] DNV GL, 2019. Class Guideline DNVGL-CG-0038: Calculation of shafts in marine applications. Accessed November 27, 2020, https://rules.dnvgl.com/docs/pdf/DNVGL/CG/2019-07/DNVGL-CG-0038.pdf.
[16] DNV GL, 2016. Class Guideline DNVGL-CG-0041: Ice strengthening of propulsion machinery. Accessed November 27, 2020, http://rules.dnvgl.com/docs/pdf/DNVGL/CG/2016-03/DNVGL-CG-0041.pdf.
[17] DNV GL, 2020. Rules for Classification: Part 6 Additional class notations, Chapter 6 Cold climate. Accessed November 27, 2020, https://rules.dnvgl.com/docs/pdf/DNVGL/RU-SHIP/2020-07/DNVGL-RU-SHIP-Pt6Ch6.pdf.
[18] Polić, D., Ehlers, S., and Æsøy, V., 2019. "Inverse modeling approach for transformation of propeller shaft angular deformation and velocity to propeller torque load". *Marine Structures,* ***67***, p. 102614.
[19] Ikonen, T., Peltokorpi, O., and Karhunen, J., 2015. "Inverse ice-induced moment determination on the propeller of an ice-going vessel". *Cold Regions Science and Technology,* ***112***, pp. 1–13.
[20] De Waal, R., Bekker, A., and Heyns, P. S., 2018. "Indirect load case estimation for propeller-ice moments from shaft line torque measurements". *Cold Regions Science and Technology,* ***151***, pp. 237–248.
[21] DNV GL, 2020. Rules for Classification: Part 4 Rotating machinery, Chapter 4 Power transmission. Accessed November 27, 2020, https://rules.dnvgl.com/docs/pdf/DNVGL/RU-SHIP/2020-07/DNVGL-RU-SHIP-Pt4Ch4.pdf.
[22] Vizentin, G., Vukelic, G., Murawski, L., Recho, N., and Orovic, J., 2020. "Marine Propulsion System Failures—A Review". *Journal of Marine Science and Engineering,* ***8***(9), p. 662.
[23] Miller, K., and Zachariah, K., 1977. "Cumulative damage laws for fatigue crack initiation and stage I propagation". *The journal of strain analysis for engineering design,* ***12***(4), pp. 262–270.
[24] Irvine, T., 2016. "Multiaxis Rainflow Fatigue Methods for Nonstationary Vibration". In Journal of Physics: Conference Series, Vol. 744, p. 012171.
[25] Frost, N. E., Marsh, K. J., and Pook, L. P., 1999. *Metal fatigue*. Courier Corporation.
[26] Garbatov, Y., and Guedes Soares, C., 2010. "Assessment of the uncertainties introduced by different fatigue damage models for ship structural details". In International Conference on Offshore Mechanics and Arctic Engineering, Vol. 49101, pp. 549–559.
[27] Nejad, A. R., Gao, Z., and Moan, T., 2014. "On long-term fatigue damage and reliability analysis of gears under wind loads in offshore wind turbine drivetrains". *International Journal of Fatigue,* ***61***, pp. 116–128.
[28] Sankararaman, S., 2015. "Significance, interpretation, and quantification of uncertainty in prognostics and remaining useful life prediction". *Mechanical Systems and Signal Processing,* ***52***, pp. 228–247.
[29] Nickerson, B. M., and Bekker, A., 2019. "Validation of external moment determination for the shaft-line of the SA Agulhas II". In International Conference on Offshore Mechanics and Arctic Engineering, Vol. 58783, American Society of Mechanical Engineers, p. V003T02A095.
[30] Han, H. S., Lee, K. H., and Park, S. H., 2016. "Parametric study to identify the cause of high torsional vibration of the propulsion shaft in the ship". *Engineering Failure Analysis,* ***59***, pp. 334 – 346.
[31] Karadeniz, H., 2001. "Uncertainty modeling in the fatigue reliability calculation of offshore structures". *Reliability Engineering & System Safety,* ***74***(3), pp. 323–335.
[32] Militaru, R., 2015. "An adaptive stepsize algorithm for the numerical solving of initial-value problems". *Analele Universitatii" Ovidius" Constanta-Seria Matematica,* ***23***(1), pp. 185–198.
[33] Anderson, K., and Daniewicz, S., 2018. "Statistical analysis of the influence of defects on fatigue life using a Gumbel distribution". *International Journal of Fatigue,* ***112***, pp. 78 – 83.
[34] Mansour, A. E., 1989. An introduction to structural reliability theory. Tech. rep., Mansour Engineering.
[35] De Waal, R. J. O., Bekker, A., and Heyns, P. S., 2018. "Data for indirect load case estimation of ice-induced moments from shaft line torque measurements". *Data in brief,* ***19***, pp. 1222–1236.
[36] DNV GL, 2003. S.A. AGULHAS II. Accessed December 29, 2020, https://vesselregister.dnvgl.com /VesselRegister/vesseldetails. htmlvesselid=30528.
[37] STX Europe, 2009. Polar Supply and Research Vessel Shaft Line Arrangement (Rev D).
[38] ASM International, 2002. *Atlas of Stress-Strain Curves*, 2 ed. ASM International.
[39] Rolls-Royce AB, 2010. Polar Research Vessel (STX NB1369): Ice impact simulation.